



**HAL**  
open science

# Photocatalytic degradation of binary and ternary mixtures of antibiotics reactive species investigation in pilot scale

H. Zeghioud, M. Kamagaté, L.S. Coulibaly, S. Rtimi, A.A. Assadi

## ► To cite this version:

H. Zeghioud, M. Kamagaté, L.S. Coulibaly, S. Rtimi, A.A. Assadi. Photocatalytic degradation of binary and ternary mixtures of antibiotics reactive species investigation in pilot scale. *Chemical Engineering Research and Design*, 2019, 144, pp.300-309. 10.1016/j.cherd.2019.02.015 . hal-02090009

**HAL Id: hal-02090009**

**<https://univ-rennes.hal.science/hal-02090009>**

Submitted on 16 Apr 2019

**HAL** is a multi-disciplinary open access archive for the deposit and dissemination of scientific research documents, whether they are published or not. The documents may come from teaching and research institutions in France or abroad, or from public or private research centers.

L'archive ouverte pluridisciplinaire **HAL**, est destinée au dépôt et à la diffusion de documents scientifiques de niveau recherche, publiés ou non, émanant des établissements d'enseignement et de recherche français ou étrangers, des laboratoires publics ou privés.

# Photocatalytic degradation of binary and ternary mixtures of antibiotics: reactive species investigation in pilot scale

Hichem Zeghioud<sup>1</sup>, Mahamadou Kamagate<sup>2,3</sup>, Lassina Sandotin Coulibaly<sup>4</sup>, Sami Rtimi\*<sup>5</sup>, Aymen Amine Assadi\*<sup>2</sup>

<sup>1</sup> Department of Process Engineering, Faculty of Engineering, Badji Mokhtar University, P.O. Box 12, 23000 Annaba, Algeria.

<sup>2</sup> Ecole Nationale Supérieure de Chimie de Rennes, UMR CNRS 6226, 11 Allée de Beaulieu, F-35708, Rennes Cedex 7, France.

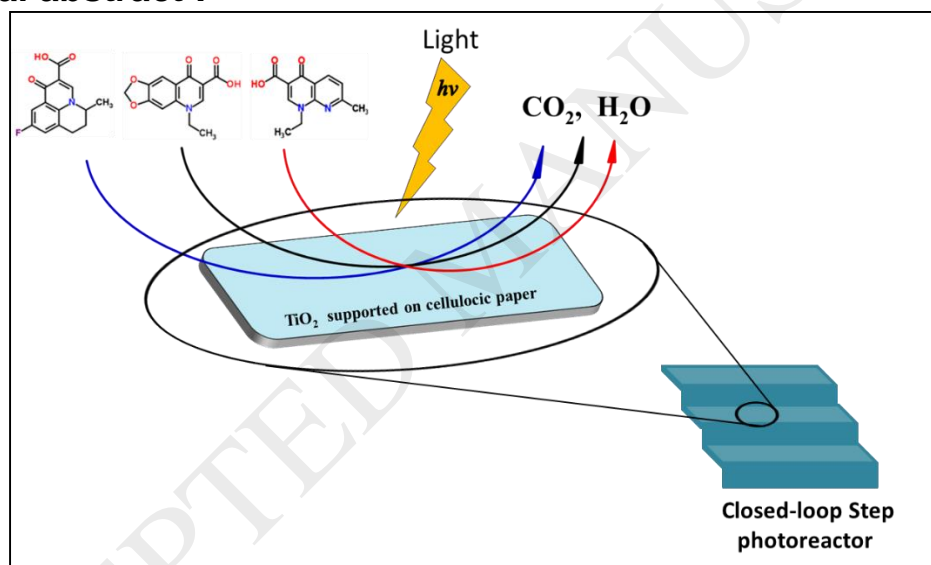
<sup>3</sup> Université Nangui Abrogoua, 02 BP 801 Abidjan 02, Cote d'Ivoire.

<sup>4</sup> Université de Man, BPV 40 Man, Côte d'Ivoire.

<sup>5</sup> Ecole Polytechnique Fédérale de Lausanne, EPFL-SB-ISIC-GPAO, Station 6, CH-1015 Lausanne, Switzerland.

\*Corresponding authors e-mail: sami.rtimi@epfl.ch and aymen.assadi@ensc-rennes.fr

## Graphical abstract :



## Highlights

- Closed-loop step photo-reactor was used for the degradation of antibiotics
- High degradation of multi-compound antibiotic solution was observed
- Rate constant of oxolinic and nalidixic acids with hydroxyl radicals was determined
- The distribution of TiO<sub>2</sub> supported on cellulose fibers was investigated with respect to SiO<sub>2</sub>

## ABSTRACT

The present study investigates the photocatalytic degradation of three quinolone antibiotics (*i.e.*, Flumequine (FLU), Oxolinic Acid (OA) and Nalidixic Acid (NA)) in mono-, binary and ternary compound systems. The closed-loop step photo-reactor and TiO<sub>2</sub> impregnated on cellulosic paper

as supported photo-catalyst in presence of UV light irradiation were used. The degradation of FLU occurred within 4 hours. A 65.4 % mineralization of OA was observed in a mono-compound system, due to the fast conversion of these main by-products formed. Besides, the investigation of the contribution of free radicals revealed the involvement of hole ( $h^+$ ),  $O_2^{\bullet-}$ , but mainly  $\bullet OH$  on the degradation of OA. The second-order kinetic rate constants calculated relative to the contribution of  $\bullet OH$  radicals on the degradation of OA was  $4.03 \times 10^9 M^{-1}s^{-1}$ , whereas for that of NA was  $4.42 \times 10^9 M^{-1}s^{-1}$ , thus underscoring that  $\bullet OH$  is the primary reactive species implicated in the photocatalytic degradation of these compounds on  $TiO_2$ /cellulosic paper catalysts. The mono-compound system shows a higher degradation rate compared to multi-compound system (binary and ternary) which explained by the competitive adsorption of antibiotics on the available active sites of photocatalyst surface. Overall, the constant photocatalytic rates are higher following this order: mono-compound system > ternary mixture > binary mixture. The catalyst was characterized by mean of FTIR, HR-TEM and XRD. The  $SiO_2$ -binder role was discussed in details based on the atomic distribution of elements on the cellulose fibers as shown by the EDS atomic mapping.

**Keywords:** Antibiotic mixture, Photocatalytic degradation, mono-compound system, Binary/Ternary compounds system, Radical Scavengers, surface characterization.

## Introduction

The growth of agri-business and aquaculture industry has been accompanied with certain practices that are potentially harmful for human and animal health. Since a decade, industrial aquaculture has quadrupled worldwide, and most of these have been followed by unrestricted use of antibiotics, turning these productive activities into a public health problem [1, 2]. Unintentional consumption of antibiotics modifies normal flora, contributing to increased susceptibility to bacterial infections. Moreover, antibiotics can also cause allergy and toxicity and lead to the development of antibiotic-resistant bacteria. Some studies reported that this resistance could be transferred to other aquatic or terrestrial bacteria [3, 4]. Thus, several previous works have emphasized antibiotics harmful environmental effects [5-8].

Quinolones such as flumequine, oxolinic acid, and nalidixic acid are commonly used in aquaculture. In particular, flumequine is one of the most widely used antibiotics in salmon farming, producing adverse environmental consequences due to its persistence in sediments for extended periods. Many techniques have been proposed to remove these kinds of pollutants, but

mainly wastewater treatment plants. Indeed, urban wastewater treatment plants (UWTPs) have proven ineffective for the removal of these pollutants, which remain in the exit effluents and thus reach the environment. Likewise, UWTPs effluents are considered to be among the main anthropogenic reservoirs where antibiotic-resistant bacteria can develop [9, 10].

To overcome this bacterial resistance phenomenon and their spread in the environment, advanced oxidation processes (AOPs) have been employed for antibiotic degradation. Thus, some authors reported amoxicillin degradation using UV-A/TiO<sub>2</sub> photocatalysis [11], as well as photo-catalytic disinfection (PCD) treatment of antibiotic sensitive (K12) and multi-drug resistant *E. coli* strains [12]. Ben et al. [13] found that quinolone antibiotics could be degraded by Ozone. Other AOPs such as electro-Fenton [14], UV photolysis and UV/H<sub>2</sub>O<sub>2</sub> [15] processes were employed to the degradation and the mineralization of ciprofloxacin, and the transformation of some antibiotics shows different structural classes. Recently, Kamagate et al. [16] reported that some antibiotics such as flumequine, norfloxacin and ciprofloxacin could be degraded simultaneously by heterogeneous photo-Fenton process using laterite as catalyst. In the case of photocatalysis, most of the researchers have assessed the performance of removal within mono-compound systems [17-19]. Otherwise, a diversity of hazardous pollutants with different concentrations coexists in the real effluents. Thus, synergistic or antagonistic effects should be taken into account regarding the performance study processes [20, 21]. Few works have been reported until now on the degradation of binary and ternary mixture of antibiotics by closed-loop step photo-reactor [22, 23].

Photocatalysis is known as AOP, which applied in both air and water purification, mainly in the case of persistent pollutants [24]. This process implies the excitation of electrons of valence band to move into the conduction band, leaving behind a positive hole ( $h^+$ ). When the latter react with the water molecules adsorbed on the catalyst surface, they generate hydroxyl radicals ( $\cdot\text{OH}$ ). The electron combines with oxygen to form the couple hydroperoxide and superoxide anions ( $\text{HO}_2\cdot$  /  $\text{O}_2\cdot^-$ ) [25, 26]. These free radicals will react with the pollutants leading to its degradation and/or mineralization [27].

In this study, the simultaneous degradation of binary and ternary mixtures of antibiotics in a continuous flow reactor, as well as the mineralization and the contribution of different reactive oxygen species (ROS) are investigated at neutral pH in order to mimic the decontamination in real environment. Before, the photocatalytic degradation efficiency of each antibiotic was studied by mean of TiO<sub>2</sub> impregnated on cellulosic fibers under UV-A light ( $\lambda_{\text{max}} = 365 \text{ nm}$ ), which normally exist in solar spectrum reaching the earth. Likewise, the mineralization of these compounds was followed. Finally, the photodegradation effect of TiO<sub>2</sub>-supported on cellulosic paper has been followed by the Infra-Red spectra and X-ray diffraction (XRD) at time of exposure to light.

## 2. Experimental

### 2.1. Materials

Carbon tetrachloride (purity > 99.8 %, R.P. Normapur), Ethylenediaminetetra-acetic acid (purity > 99 wt. %, Prolabo), Chloroform (99.97 %, Acros-Organics) were used. Flumequine (FLU), Oxolinic Acid (OA) and Nalidixic Acid (NA), Hydrochloric acid (HCl, 37 % v/v), 2-Propanol (purity > 99.5 %), Sodium hydroxide (NaOH, 98 % purity) were purchased from Sigma–Aldrich in France. Stock solutions were prepared with high-purity water obtained from a Millipore Milli-Q system with a resistivity of 18.2 M $\Omega$  cm<sup>2</sup>. Physico-chemical properties of antibiotics and its structures are shown in Table 1.

### 2.2. Characterization of the catalyst

Titanium dioxide (PC-500, 85% Anatase, crystallites mean size = 5 -10 nm) was coated using of a binder on non-woven paper formed by natural cellulose fibers (2 mm thick). The used binder was an aqueous dispersion of colloidal SiO<sub>2</sub>. The coating of the cellulose fibers consists of a mixture of TiO<sub>2</sub> and SiO<sub>2</sub> nanoparticles (mass ratio = 1) with average size distribution of 25 nm. A careful washing of the coating was carried after the deposition in order to remove the unbounded or weakly bonded TiO<sub>2</sub>. The remaining TiO<sub>2</sub> load on the surface was 25 g/m<sup>2</sup>. In the next sections

of the study, the combined system:  $\text{TiO}_2 + \text{SiO}_2 +$  the cellulose fibers will be referred to as the photocatalyst [28].

To understand whether the  $\text{TiO}_2$ -supporting cellulose fibers remained unchanged after treatment in case of long-time exposure to light, attenuated total reflectance-Fourier transform infrared (ATR-FTIR) spectra were carried out between in the  $650\text{-}4000\text{ cm}^{-1}$  region on an IS50 Nicolet spectrometer equipped with a KBr beam splitter and a TCD detector. A nine-reflection diamond ATR accessory (DurasamplIR™, SensIR Technologies) was used for acquiring spectra of wet samples. The resolution of the single beam spectra was  $4\text{ cm}^{-1}$ .

X-ray diffractograms (XRD) have been also performed using a Philips PW1830X-ray diffractometer in a Bragg Brentano configuration to identify the crystal phase and structure. The observed patterns have been determined using Philips X'Pert High Score software and compared with standard patterns of International Center of Diffraction Data (ICDD) databases.

For TEM analysis, the coated cellulosic fibers were embedded in epoxy then cut with ultra-microtome into thin layers with thickness of 80-100 nm. These layers were placed on TEM holey carbon grid. FEI Osiris microscope was used for imaging and operated at 200 kV, with spot size of 5, dwell time  $50\ \mu\text{s}$  and real time 600s.

### 2.3. Photocatalytic experiments

The photocatalytic degradation of the mono-, bi and tri-compound systems were carried out in a closed-loop step photo-reactor. The photo-reactor includes three lamps Philips Bulb lamp emitting a UV-A light (24 W UVA;  $\lambda_{\text{max}} = 365\text{ nm}$ ), a Gear Pump Drive 75211-15 operating at a flow rate of  $125\text{ L h}^{-1}$ , a tank of 2 L capacity with magnetic stirrer, and the  $\text{TiO}_2$  impregnated on cellulosic fibers as photo-catalyst (Fig.1). For the experiment, 1.5 L of each solution (FLU, NA and OA) of known concentration (*i.e.*,  $5\text{ mg L}^{-1}$ ) was prepared and recirculated. The pH of the solution was adjusted by HCl and NaOH (0.01M). The solution was recirculated in the dark for 45 min to reach

adsorption equilibrium before irradiation. At time intervals, 5 mL of the solution was collected and analyzed.

#### 2.4. Sample analysis

Aqueous concentrations of FLU, NA, and OA were determined using a high-performance liquid chromatography (Waters 600 Controller) equipped with a reversed-phase C18 column (250 mm×4.6 mm i.d., 5 μm) and UV detector (Waters 2489). The detector was set to 246, 258, 268 nm for FLU, NA, and OA, respectively. The mobile phase was a mixture of acetonitrile/water (40/60 v/v) with 0.1 % formic acid. The flow rate was set at 1 mL min<sup>-1</sup> in isocratic mode. Under these conditions, the retention times of FLU, NA, and OA were 6.5, 5.8 and 5 min, respectively. Total Organic Carbon (TOC) was determined using a TOC-meter (Shimadzu TOC-VCSH). The scavenging experiments were performed using 5 mg L<sup>-1</sup> of; Isopropanol, carbon tetrachloride or chloroform and EDTA to determine the contributions of O<sub>2</sub><sup>•-</sup>, hole (h<sup>+</sup>) and •OH within the degradation of these three antibiotics, respectively. The degradation efficiency (%) was estimated using Eq 1.

$$\eta(\%) = \left( \frac{C_0 - C_t}{C_0} \right) \times 100 \quad (1)$$

where, C<sub>0</sub> and C<sub>t</sub> are the initial concentration and the concentration at time *t* of antibiotic, respectively.

Then, the mineralization yield was calculated according to the Eq 2.

$$\text{Mineralization yield (\%)} = \left( \frac{TOC_0 - TOC_t}{TOC_0} \right) \times 100 \quad (2)$$

where, TOC<sub>0</sub> and TOC<sub>t</sub> are the initial Total Organic Carbon and the Total Organic Carbon at time *t*, respectively.

#### 2.5. Determination of second-order rate constant of some compounds reacting with •OH radicals

The second-order rate constant between •OH radicals and some compounds (*i.e.*, oxolinic acid (OA) and nalidixic acid (NA)) reaction was determined by Parker et al. [29] and Boreen et al. [30]

methods. Flumequine (FLU) with a known  $^{\bullet}\text{OH}$  rate constant ( $k_{\text{OH, FLU}} = 8.26 \times 10^9 \text{ M}^{-1}\text{s}^{-1}$ ) [31], was used as the reference compound (R) in this study.

### 3. Results and discussion

#### 3.1. Degradation efficiency of closed-loop step photo-reactor

Figure 2 shows the degradation efficiencies of FLU, OA and NA versus time. In fact, a complete degradation was obtained for all the compounds within 240 min. It is worthy to note that the degradation of FLU was much faster, followed by that of NA, while OA degradation was the slowest. This result can be explained by the fact that OA has a major hemolytic effect and is more photo-stable than FLU and NA [32, 33]. Hidalgo et al. [32] reported on the photostability of some pharmaceutical compounds, which decreased in the order: oxolinic acid (OA) > rosoxacin (RS) > M-193324 > nalidixic acid (NA) > pipemidic acid (PA) > norfloxacin (NF) > ciprofloxacin (CP). This study showed that nalidixic acid (NA) is less photo-stable compared to oxolinic acid (OA), which can justify the faster degradation of NA. Regarding FLU, Sirtori et al. [34] found the same degradation trend with NA during 25 min of illumination in presence of  $\text{TiO}_2\text{-P25}$  (Degussa) in suspension.

When using  $\text{TiO}_2$  in suspension, separation and filtration of the catalyst at the end of the process is necessary for the catalyst reuse. For this reason, our study focuses on the degradation of pollutants on supported  $\text{TiO}_2$  on cellulosic paper. Herrington and Midmore, 1984, were the first to report that the primary origin of the charge on cellulose fibers is the dissociation of carboxylic acid groups on their surface [35]. Two main acid groups with pK values of 4.0 and 9.2 were reported for cellulose fibers. The former was concluded to be a C6 carboxy-group as oxycellulose; the latter pK was thought to be ammonia as an impurity, especially existing on natural cellulosic fibers. This confers polar groups  $\text{COO}^-$  and  $\text{OH}^+$  able to bind  $\text{TiO}_2$  with its different polarities. In principle, equilibrium of the acid/base groups on the  $\text{TiO}_2$  interface may be assumed even if the crystal structure is not stable. During the photocatalytic degradation of the mono-, bi- or tri-

compound system, the TiO<sub>2</sub>/wastewater solution interface is dominated by the properties of ≡TiOH<sup>1/3-</sup> and ≡OH<sup>1/3+</sup> surface groups [36]. The acid–base character of these polar sites is represented by the two interfacial equilibria shown in eq.3 and eq. 4 below:



The rapid degradation of FLU at the beginning reaction can be due to the supported catalyst used in this study showing polar groups able to facilitate the contact with the pollutant. Vaizoğullar [37] tested several catalysts and showed that the supported catalysts improved the FLU degradation.

The pKa of flumequine is higher than typical carboxylic acids (6.27). This because of the stabilization proton by hydrogen bonding to the adjacent =O group. This allows polarity of the TiO<sub>2</sub>-cellulosic paper catalyst interacting with the surrounding FLU (or other pollutant) molecules leading to their adsorption and thus their oxidation.

### 3.2. Mineralization of mono-compound systems

With the aim, TOC measurements were performed to follow the mineralization of each antibiotic during photo-catalytic treatment. As it is readily seen in Fig.3a, a progressive increase of the pollutants mineralization and consequently a progressive TOC reduction over time were observed. We noted 65.4 % of OA mineralization, whereas those of FLU and NA achieved 57.3 % and 43.4 % after 6 h on the supported TiO<sub>2</sub> under light, respectively. This fast OA mineralization suggests that photocatalysis with TiO<sub>2</sub> is efficient in rapidly converting this antibiotic into non-toxic by-products [38, 39]. Indeed, Giraldo et al. [38] showed that the aromatic intermediates were formed within the 45 min of treatment. Unlike OA, FLU mineralization occurred after its degradation within 180 min of UV illumination, while the mineralization of NA began after 60 min (before total degradation). The same trends were obtained by Sirtori et al. [34], following FLU and NA mineralization by TiO<sub>2</sub> suspensions. Indeed, the generated reactive oxygen species (ROS) could

be firstly consumed by the fragments of FLU, and then broken down into by-products, and finally CO<sub>2</sub> and H<sub>2</sub>O and other minerals. Otherwise, the mineralization of OA and NA was occurred simultaneously with their degradation, thus showing that the generated ROS were consumed directly by their fragments as well as by-products leading to mineralization. However, the mineralization of OA, NA, and FLU in individually solutions could be described by Pseudo-first-order kinetics [40]. A good linear correlation between  $\ln(\text{TOC}_0/\text{TOC})$  versus time according to the regression coefficient ( $R^2$ ) (*i.e.*, 0.998, 0.979 and 0.939 for OA, NA and FLU, respectively) was observed. The comparison between Pseudo-first-order constant ( $k'$ ) of mineralization rate for different antibiotics in mono-component system is presented in Fig.3b. The mineralization rate ( $k'$ ) of OA ( $28.8 \cdot 10^{-4} \pm 10^{-4} \text{ min}^{-1}$ ) is higher than those of FLU ( $17.4 \cdot 10^{-4} \pm 10^{-5} \text{ min}^{-1}$ ) and NA ( $13.7 \cdot 10^{-4} \pm 10^{-5} \text{ min}^{-1}$ ).

### 3.3. Effect of different scavengers on OA degradation

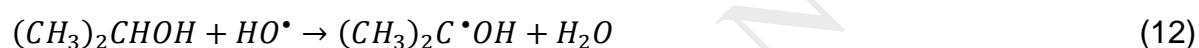
The photocatalytic reaction starts by absorbing UV photons with the formation of electron-hole pairs ( $e^-/h^+$ ) on the surface of TiO<sub>2</sub> by following equation 5 [26].



Moreover, H<sub>2</sub>O and O<sub>2</sub> molecules could transfer electrons from holes valence band towards conduction band to produce  $\bullet\text{OH}$  by following these chain reactions [41]. Then, these different radicals would react with OA.



To understand the involvement of these active radicals upon the photocatalysis process, EDTA, isopropyl alcohol and chloroform ( $\text{CHCl}_3$ ) were used as scavengers of hole ( $h^+$ ),  $\cdot\text{OH}$  and  $\text{O}_2^{\bullet-}$ , respectively [42- 45]. It is worth to mention at this stage that At pH  $\sim 6$ , the photocatalytic degradation and/or mineralization of OA would preferentially proceed via the predominant  $\text{O}_2^{\bullet-}$  species over  $\text{HO}_2^{\bullet-}$ . The effect of these different radical acceptors on the OA degradation and their constant rate were shown in Fig.4. In the presence of iso-propanol, the degradation efficiency of OA markedly dropped from 100 % to 25 % (*i.e.*, 75 % of OA degradation was inhibited) with a constant rate of  $0.0012 \text{ min}^{-1}$ , thus underscoring that  $\cdot\text{OH}$  radicals were mainly implicated in OA degradation. Indeed, Iso-Pro has been reported as one of the best  $\cdot\text{OH}$  radical scavengers due to its high rate constant ( $k_{\text{Iso-pro}, \cdot\text{OH}} = 1.9 \times 10^9 \text{ M}^{-1}\text{s}^{-1}$ ) [43] by abstraction of the H-atom attached to the tertiary carbon of Iso-Pro as shown in equation 12 below [46,47].



When the same concentration of EDTA was added, OA degradation efficiency inhibition was low ( $\sim 25\%$ ) leading to 65% OA degradation inhibition with a constant rate of  $0.0036 \text{ min}^{-1}$ , whereas when adding  $\text{CHCl}_3$ , 40 % of inhibition (*i.e.*, from 100 % to 60 % of degradation) was obtained with a constant rate of  $0.0024 \text{ min}^{-1}$ , suggesting a minor contribution of the photo-generated holes in the process of pollutant degradation conversely  $\text{O}_2^{\bullet-}$ . In conclusion, the order of implication of each photo-generated active species can be as follow: hole ( $h^+$ ) followed by a low contribution of  $\text{O}_2^{\bullet-}$  and the main contribution is attributed to  $\cdot\text{OH}$  for the OA degradation in the mono-compound system.

### 3.4. Estimation of the second-order rate constants between organic compounds and the photo-generated $\cdot\text{OH}$ radicals

The reaction between  $\cdot\text{OH}$  radicals and organic ligand (S) follows a second order kinetic. This decay rate can be expressed by the following equation:

$$-(d[S])/dt = [k_{\cdot\text{OH}, \text{S}}][\cdot\text{OH}][S] \quad (13)$$

Where  $[k_{\bullet\text{OH}, S}]$  is the second order constant rate for the reaction between S and  $\bullet\text{OH}$ . Indeed, the reaction of hydroxyl radicals generation represents the limiting step in the oxidation of most organic compounds, due to the slower rate of this reaction compared to the consumption of  $\bullet\text{OH}$  radicals by organic compounds and the formation of the by-products [48,49]. By assuming constant the  $\bullet\text{OH}$  radical's concentration in the solution, the rate of the reaction can be described by pseudo-first-order model relative to the concentration of organic compounds:

$$-(d[\bullet\text{OH}])/dt = 0 \quad (14)$$

$$-(d[S])/dt = k_{app}[S] \quad (15)$$

This can be ascribed as:

$$\ln\left(\frac{S_t}{S_0}\right) = -k_{app} \cdot t \quad (16)$$

$$\text{with } k_{app} = [k_{\bullet\text{OH}, S}][\bullet\text{OH}] \quad (17)$$

Experimentally, monitoring of the organic compound (S) decay versus time allows estimating the apparent rate constant of the reaction according to pseudo-first-order model. Then, the rate constant absolute of second-order of the reaction between  $\bullet\text{OH}$  radicals and organic compounds can be determined by the competitive kinetic methods, by setting competition constant  $k_s$  of the substrate (S) determined with a reference compound (R) whose kinetic constant is known [29,30]. Therefore, the different concentrations over time are given by:

$$-(d[R])/dt = [k_{\bullet\text{OH}, R}][\bullet\text{OH}][R] \quad (18)$$

Then, the equations (13) and (18) allow for writing those from below:

$$\ln([S]_0/[S]_t) = k_{(\bullet\text{OH}, S)}/k_{(\bullet\text{OH}, R)} \times \ln([R]_0/[R]_t) \quad (19)$$

This method is used in this study to estimate the second-order reaction of oxolinic acid (OA) and nalidixic acid (NA) reacting with  $\bullet\text{OH}$  using flumequine (FLU) as a reference compound ( $k_{\bullet\text{OH}, \text{FLU}} = 8.26 \times 10^9 \text{ M}^{-1}\text{s}^{-1}$ ). Thus, equation 19 leads to equation 20 below:

$$\ln([OA \text{ or } NA]_0/[OA \text{ or } NA]_t) = k_{(\bullet\text{OH}, OA \text{ or } NA)}/k_{(\bullet\text{OH}, \text{FLU})} \times \ln([FLU]_0/[FLU]_t) \quad (20)$$

The reaction rate constants were estimated by plotting  $\ln([\text{OA or NA}]_0/[\text{OA or NA}]_t)$  versus  $\ln([\text{FLU}]_0/[\text{FLU}]_t)$  as shown in **Fig. 5**. The results obtained for OA (*i.e.*,  $k_{\bullet\text{OH}, \text{OA}}$ ) was  $4.03 \times 10^9 \text{ M}^{-1}\text{s}^{-1}$ , whereas of that of NA (*i.e.*,  $k_{\bullet\text{OH}, \text{NA}}$ ) was  $4.42 \times 10^9 \text{ M}^{-1}\text{s}^{-1}$ . These high values for the second-order kinetic rate constant confirms that  $\bullet\text{OH}$  is the primary reactive species involved in the photocatalytic degradation of these compounds on  $\text{TiO}_2/\text{cellulosic fiber}$  catalysts.

### 3.5. Degradation efficiencies in binary and ternary systems

Figure 6 shows the simultaneous degradation efficiencies of FLU, OA and NA versus time. For the simultaneous degradation of FLU with OA or NA, we noted higher degradation efficiencies regarding FLU relatively to both during the photocatalysis process. These results could be explained by the fact that  $\bullet\text{OH}$  radicals were strongly involved within degradation of these compounds, and that the second order rate constant of FLU with  $\bullet\text{OH}$  was higher than those of both OA and NA as estimated above in Fig.5. According to Santoke et al. [31], the second order rate constant of FLU with  $\bullet\text{OH}$  is  $k_{\bullet\text{OH}, \text{FLU}} = 8.26 \times 10^9 \text{ M}^{-1}\text{s}^{-1}$ , whereas those of OA and NA were  $4.03 \times 10^9 \text{ M}^{-1}\text{s}^{-1}$  and  $4.42 \times 10^9 \text{ M}^{-1}\text{s}^{-1}$ , respectively. On the other hand, a high degradation efficiency of NA versus OA during their simultaneous degradation could be due to a high second order rate constant of NA, unlike OA. Despite the high mineralization rate of OA in the mono-compound system, it holds that the degradation efficiency in binary system confirms those of mono-compound systems, which is lower than those of NA and FLU. Hidalgo et al. [32] investigated also the photodegradable behavior of some quinolones and found that OA was very photo-stable. Otherwise, in the ternary system, we noted firstly high degradation percentages of NA at the beginning of the reaction (*i.e.*, from 30 to 90 min), then, this degradation percentage became similar at those of FLU until 240 min and decreased after 300 min under light. Similar trend was observed by Sirtori et al. [34], which could be attributed of a competition of the by-products formed during FLU or NA decomposition and these mother compounds on the  $\text{TiO}_2$  surface (in mono-compound systems). In our study, the competition is stronger since it lies between the supported  $\text{TiO}_2$  surface and the 3 mother compounds associated with their by-

products, which makes the system more complex mimicking a hospital wastewater effluent. In a real set, the competitive interaction of TiO<sub>2</sub> surface and the existing compounds can be influenced by: (i) the pH of the media and its evolution during the photocatalytic process (ii) the charge/polarity of the compounds, and (iii) the differences of concentration of each compound leading to different by-products concentrations.

### 3.6. Degradation rates and radicals contribution percentages of multi-compound in different systems

The photocatalytic degradation of FLU, OA and NA antibiotics could be described by the pseudo-first-order kinetics following the slope of the straight-line plot of  $\ln(C_0/C)$  versus time (min):

$$\ln \left( \frac{C_0}{C_t} \right) = k \cdot t \quad (21)$$

where,  $C_0$  and  $C_t$  are the initial and residual concentrations ( $\text{mg L}^{-1}$ ) of the treated solution at the instant  $t$  of photocatalytic reaction, respectively.

The Pseudo-first-order rate constant values decreased in the mono-component system following this order:  $k_{\text{FLU}} > k_{\text{NA}} > k_{\text{OA}}$ . The  $k_{\text{FLU}}$  value was  $0.017 \text{ min}^{-1}$  in mono-compound system, which dropped nearly 3-fold in binary systems (*i.e.*,  $k = 0.0055 \text{ min}^{-1}$ ) and 2-fold in ternary systems (*i.e.*,  $k = 0.009 \text{ min}^{-1}$ ); whereas those of OA decreased just about 2-fold in both system (*i.e.*,  $k = 0.0035 \text{ min}^{-1}$  in binary system and  $0.0045 \text{ min}^{-1}$  in ternary). In the case of NA, the decrease of  $k$  values from mono-compound system to multi-compound system depended on the combination of the molecules and the systems. We observed a decrease of about 2-fold and 3-fold in presence of OA and FLU, respectively, while that in ternary was 1.4-fold (*i.e.*, NA/FLU/OA system). This inhibition could be due to the competitive adsorption of two antibiotics and their by-products on the available active sites of the catalyst surface where the molecule size and functional groups play a crucial role [34]. Likewise, a slight increase of  $k$  in the ternary system compared to the binary system for all the three antibiotics was observed, but the degradation efficiencies remained less than those of binary system. It is worthy to note that radicals contribution determined varied

versus the different compound systems. Indeed, high contribution of  $O_2^{\bullet-}$  was observed upon FLU degradation, while for AO and NA,  $\cdot OH$  contribution was higher in the mono-compound system. In the binary system as well as in the ternary system,  $O_2^{\bullet-}$  and  $\cdot OH$  contributed widely, except in the system OA + NA, where  $\cdot OH$  dominated.

### 3.7. Characterization of the photocatalytic surface:

#### 3.7.1. TEM imaging and elements distribution/mapping

Figure 8a shows the HAADF distribution of the  $TiO_2/SiO_2$  coating on the fibrous cellulose fabrics. It is readily seen from Figure 8a that the coating is well distributed along the cellulose fibers with respect to the Ti/Si ratio of 1 as reported in the experimental section. Figure 8b shows that the  $SiO_2$  binder plays a role for the distribution of  $TiO_2$  leading to enhanced adhesion to the cellulose substrate. The  $SiO_2$  binder tightly bonds the particles leading to the formation of the compact layer as shown in Figure 8a. In addition to the bridging role, the binder may serve to alleviate the stresses of Ti nanoparticles resulting from the volume change during the catalyst preparation. The  $SiO_2$  encompass  $TiO_2$  leading to the formation of  $TiO_2$ -islands. Figure 8b shows the anastomosing behavior of  $SiO_2$  forming micro-sized aggregates of  $TiO_2$  on the cellulose fiber surface.

#### 3.7.2. FTIR spectra

To study the stability of the supported catalyst after the antibiotics degradation, IR spectra of the  $TiO_2$ -supporting cellulosic fibers before and after the photocatalytic treatment were carried out and the results are shown in Figure 9. As shown in the Figure 9, the spectrum of the virgin  $TiO_2$ /cellulose catalyst is characterized by an intense and broad band in the  $3600-3100\text{ cm}^{-1}$  range, associated with inter- and intra-chain OH-O groups of the interacting chains, and a peak at  $1700-1600\text{ cm}^{-1}$  is also indicative of the presence of interstitial or adsorbed water [50, 51]. Thus, a strong broad band at  $691\text{ cm}^{-1}$  was attributed to the stretching vibration of Ti-O-Ti for  $TiO_2$  samples [52, 53]. We also noted the adsorption of quinolone between  $1100-1000\text{ cm}^{-1}$  and  $1600-1700\text{ cm}^{-1}$  compared to the virgin  $TiO_2$ /cellulose catalyst. A higher intensity at  $1638\text{ cm}^{-1}$  and  $1073\text{ cm}^{-1}$  was observed for ternary compound system photodegradation. This peak can be

attributed to the further  $\text{-C=O}$  and  $\text{-C-O}$  stretching vibration of antibiotics [54, 55]. These findings proved that a high adsorption of antibiotics onto the surface of the photocatalyst would be beneficial for the photodegradation.

### 3.7.3. XRD patterns

Figure 10 shows the XRD patterns of  $\text{TiO}_2$ /cellulose catalyst in presence of FLU, FLU + NA and FLU + NA + OA. The peaks at  $20.3^\circ$  and  $21.8^\circ$  are corresponding to the (110) and (200) planes of crystalline cellulose, respectively. It is noted that in addition to the peaks of cellulose, the  $\text{TiO}_2$  crystalline peaks such as anatase and rutile crystalline disappeared in the  $\text{TiO}_2$ /cellulose composite fiber. This can be attributed to the high intensity of the peaks attributed to the cellulose predominating the peaks assigned to  $\text{TiO}_2$  crystalline structures.

## 4. Conclusion

In the current study, the photocatalytic degradation of three antibiotics (*i.e.*, FLU, OA, and NA) was successfully performed using closed-loop step photo-reactor including  $\text{TiO}_2$  impregnated on cellulosic paper under UV irradiation. We noted a rapid degradation of FLU and a high mineralization of OA with 65.4 % in the mono-compound system. This was attributed to the fast conversion of OA into the two major by-products easily oxidized. Besides, the investigation of the contribution of the photo-generated free radicals revealed the involvement of the hole ( $h^+$ ), and  $\text{O}_2^{\cdot-}$ , but mainly  $\cdot\text{OH}$  on OA degradation. The second-order kinetic rate constants relative to the photo-generated  $\cdot\text{OH}$  were determined for OA at  $4.03 \times 10^9 \text{ M}^{-1}\text{s}^{-1}$ , whereas that of NA was  $4.42 \times 10^9 \text{ M}^{-1}\text{s}^{-1}$ . These high values confirm that  $\cdot\text{OH}$  is the primary reactive species involved in the photocatalytic degradation of these antibiotics on  $\text{TiO}_2$ /cellulosic fiber catalysts. The mono-compound system shows a higher degradation rate compared to multi-compound systems (binary and ternary) which was explained by the competitive adsorption of antibiotics on the available active sites of photocatalyst surface. TEM imaging and atomic mapping showed that the coating is well distributed on the cellulosic fibers. The  $\text{SiO}_2$  binder played a role in the distribution of  $\text{TiO}_2$

and enhanced its adhesion to the substrate leading to tightly bonded particles. The stretching vibration bonds of Ti–O–Ti were observed by FTIR. XRD results showed the presence of Anatase TiO<sub>2</sub>, but the peaks of the cellulosic substrate were predominant. Finally, TiO<sub>2</sub> impregnated on cellulosic paper under UV irradiation could be an alternative solution to antibiotic multi-compound degradation in real hospital wastewater effluents. The catalyst surface was characterized by the mean of HR-TEM, FTIR and XRD.

### **Acknowledgments**

This work was supported by Department of Process Engineering, Faculty of Engineering, Badji Mokhtar University, Algeria. S.R. thanks EPFL.

ACCEPTED MANUSCRIPT

## References

- [1] B.Y. Liu, X. P. Nie, W.Q. Liu, P. Snoeijs, C. Guan, M.T. Tsui, Toxic effects of erythromycin, ciprofloxacin and sulfamethoxazole on photosynthetic apparatus in *Selenastrum capricornutum*, *Ecotoxicol. Environ. Sa.* 74 (2011) 1027–1035.
- [2] *Resolution WHA 68-7 (Global Action Plan on Antimicrobial Resistance) of the sixty-eighth World Health Assembly, Geneva, Switzerland, 26 May, 2015.* [http://apps.who.int/gb/ebwha/pdf\\_files/WHA68/A68\\_R7-en.pdf?ua=1](http://apps.who.int/gb/ebwha/pdf_files/WHA68/A68_R7-en.pdf?ua=1). Accessed 20 May 2018.
- [3] G. Rigos, I. Nengas, M. Alexis, G. M. Troisi, Potential drug (oxytetracycline and oxolinic acid) pollution from Mediterranean sparid fish farms, *Aquatic Toxicol.* 69 (2004) 281-288.
- [4] L. Hong-Tih, C. Yew-Hu, L. Juo-Shan, Long-term transformation of oxolinic acid in water from an eel pond. *Aquaculture* 275 (2008) 96-101.
- [5] D. W. Kolpin, E. T. Furlong, M. T. Meyer, E. M. Thurman, S. D. Zaugg, L. B. Barber, H. T. Buxton, Pharmaceuticals, hormones, and other organic wastewater contaminants in US streams, 1999–2000: A national reconnaissance, *Environ. Sci. Technol.* 36 (6) (2002) 1202-1211.
- [6] X. Van Doorslaer, J. Dewulf, H. Van Langenhove, K. Demeestere, Fluoroquinolone antibiotics: An emerging class of environmental micropollutants, *Sci. Total Environ.* 500-501 (2014) 250–269.
- [7] D. Fatta-Kassinos, S. Meric, A. Nikolaou, A. Pharmaceutical, residues in environmental waters and wastewater: Current state of knowledge and future research, *Anal. Bioanal. Chem.* 399 (1) (2011) 251-275.
- [8] M. D. Hernando, M. Mezcuca, A. R. Fernández-Alba, D. Barceló, Environmental risk assessment of pharmaceutical residues in wastewater effluents, surface waters and sediments, *Talanta* 69 (2) (2006) 334-342.
- [9] I. Michael, L. Rizzo, C. S. McArdell, C. M. Manaia, C. Merlin, T. Schwartz, C. Dagot, D. Fatta-Kassinos, Urban wastewater treatment plants as hotspots for the release of antibiotics in the environment: A review, *Water Res.* 47 (2013) 957-995.
- [10] A. Novo, C.M. Manaia, Factors influencing antibiotic resistance burden in municipal wastewater treatment plants, *Appl. Microbiol. Biot.* 87(2010) 1157-1166.
- [11] D. Dimitrakopoulou, I. Rethemiotaki, Z. Frontistis, N. P. Xekoukoulotakis, D. Venieri, D. Mantzavinos, Degradation, mineralization and antibiotic inactivation of amoxicillin by UV-A/TiO<sub>2</sub> photocatalysis, *J. Environ. Manage.* 98 (2012) 168-174.
- [12] P.S.M. Dunlop, M. Ciavola, L. Rizzo, D.A. McDowell, J.A. Byrne, Effect of photocatalysis on the transfer of antibiotic resistance genes in urban wastewater, *Catal. Today* 240 (2015) 55–60.
- [13] W. Ben, Z. Qiang, P.E. M. ASCE, X. Pan, Y. Nie, Degradation of Veterinary Antibiotics by Ozone in Swine Wastewater Pretreated with Sequencing Batch Reactor, *J. Environ. Eng.* 138 (3) (2012) 272-277.
- [14] Y. Chen, A. Wang, Y. Zhang, R. Bao, X. Tian, J. Li, Electro-Fenton degradation of antibiotic ciprofloxacin (CIP): Formation of Fe<sup>3+</sup>-CIP chelate and its effect on catalytic behavior of Fe<sup>2+</sup>/Fe<sup>3+</sup> and CIP mineralization, *Electrochim. Acta* 256 (2017) 185-195.
- [15] O.S. Keen, K.G. Linden, Degradation of Antibiotic Activity during UV/H<sub>2</sub>O<sub>2</sub> Advanced Oxidation and Photolysis in Wastewater Effluent, *Environ. Sci. Technol.* 47 (2013) 13020–13030.
- [16] M. Kamagate A. A. Assadi, T. Kone, L. Coulibaly, K. Hanna Activation of persulfate by irradiated laterite for removal of fluoroquinolones in multi-component systems, *J. Hazard. Mater.* 346 (2018) 159–166.

- [17] H. Zeghioud, N. Khellaf, H. Djelal, A. Amrane, M. Bouhelassa, Photocatalytic Reactors Dedicated to the Degradation of Hazardous Organic Pollutants: Kinetics, Mechanistic Aspects and Design-A Review, *Chem. Eng. Commun.* 203 (2016) 1415–1431.
- [18] W. Lou, A. Kane, D. Wolbert, S. Rtimi, A. A. Assadi, Study of a photocatalytic process for removal of antibiotics from wastewater in a falling film photoreactor: Scavenger study and process intensification feasibility. *Chemical Engineering and Processing: Process Intensification* (2017) 122, 213-221.
- [19] C. Rodrigues-Silva, M. G. Maniero, S. Rath, J. R. Guimarães, Degradation of flumequine by photocatalysis and evaluation of antimicrobial activity, *Chem. Eng. J.* 224 (2013) 46–52.
- [20] S. Gharib-Abou Ghaida, A. A. Assadi, G. Costa, A. Bouzaza, D. Wolbert, Association of surface dielectric barrier discharge and photocatalysis in continuous reactor at pilot scale: Butyraldehyde oxidation, by-products identification and ozone valorization, *Chemical Engineering Journal*, 292, 15 (2016) 276-283
- [21] O.-M. Min, L.-N. Ho, S.-A. Ong, Y.-S. Wong, Comparison between the photocatalytic degradation of single and binary azo dyes in TiO<sub>2</sub> suspensions under solar light irradiation, *J. Water Reuse Desal.* 5(4) (2015) 579-591.
- [22] A.M. Peiro, J.A. Ayllon, J. Peral, X. Domenech, TiO<sub>2</sub>-photocatalyzed degradation of phenol and ortho-substituted phenolic compounds, *Appl. Catal. B: Environ.* 30 (2001) 359–373.
- [23] Anh Thu Nguyen, Ruey-Shin Juang, Treatment of o-Cresol/4-chlorophenol binary mixtures in aqueous solutions by TiO<sub>2</sub> photocatalysis under UV irradiation, *Desalin. Water Treat.* 57:15 (2016) 6820-6828.
- [24] Y. Belaïssa, D. Nibou, A.A. Assadi, B. Bellal, M. Trari, A new hetero-junction p-CuO/n-ZnO for the removal of amoxicillin by photocatalysis under solar irradiation, *Journal of the Taiwan Institute of Chemical Engineers*, 68 (2016) 254-265
- [25] V. Etacheri, C. D. Valentin, J. Schneider, D. Bahnemann, S.C. Pillai, Visible-light activation of TiO<sub>2</sub> photocatalysts: Advances in theory and experiments, *J. Photochem. Photobiol. C: Photochem. Rev.* 25 (2015) 1–29.
- [26] I.A. Shkrob, M.C. Jr, Sauer, Hole scavenging and photo-stimulated recombination of electron-hole pairs in aqueous TiO<sub>2</sub> nanoparticles, *J. Phys. Chem. B.* 108 (2004) 12497–12511.
- [27] R. P. Cavalcante, R. F. Dantas, B. Bayarri, O. González, J. Giménez, S. Esplugas, A.M. Junior, Photocatalytic mechanism of metoprolol oxidation by photocatalysts TiO<sub>2</sub> and TiO<sub>2</sub> doped with 5% B: Primary active species and intermediates, *Appl. Catal. B: Environ.* 194 (2016) 111–122.
- [28] D. Chebli, F. Fourcade, S. Brosillon, S. Nacef, A. Amrane, Integration of photocatalysis and biological treatment for azo dye removal – application to AR183, *Environmental Technology*, 32:5(2011) 507-514,
- [29] J. L. Packer, J.J. Werner, D. E. Latch, K. McNeill, W. A. Arnold, Photochemical fate of pharmaceuticals in the environment: Naproxen, diclofenac, clofibrac acid, and ibuprofen, *Aquat. Sci.* 65 (2003) 342–351.
- [30] A. Boreen, W. A. Arnold, K. McNeill, Photochemical Fate of Sulfa Drugs in the Aquatic Environment: Sulfa Drugs Containing Five-Membered Heterocyclic Groups, *Environ. Sci. Technol.* 38 (2004) 3933-3940.
- [31] H. Santoke, W. Song, W.J. Cooper, J. Greaves, G.E. Miller, Free-radicals-Induced oxidative and reductive degradation of fluoroquinolone pharmaceuticals: Kinetic studies and degradation mechanism, *J. Phys. Chem. A* 113 (2009) 7846-7851.
- [32] M. E. Hidalgo, C. Pessoa, E. Fernández, A. M. Cárdenas, Comparative determination of Quinolones, *J. Photochem. Photobiol. A: Chem.* 73 (1993) 135-138.
- [33] F. Vargas, C. Rivas, Mechanistic Studies On Phototoxicity Induced By Antibacterial Quinolones, *Toxic Subst. Mech.*, 16(1) (1997) 81-86.

- [34] C. Sirtori, A. Zapata, S. Malato, W. Gernjak, A. R. Fernández-Alba, A. Agüera, Solar photocatalytic treatment of quinolones: intermediates and toxicity evaluation, *Photochem. Photobiol. Sci.* 8 (2009) 644–651.
- [35] M. T. Herrington, B. R. Midmor, Adsorption of Ions at the Cellulose/Aqueous Electrolyte Interface Part 1. Charge/pH Isotherms, *J. Chem. Soc., Faraday Trans. I*, 80 (1984), 1525-1537.
- [36] R. Rodriguez, M. A. Blesa, and A. E. Regazzoni, Surface complexation at the TiO<sub>2</sub> (anatase) /aqueous solution interface: chemisorption of catechol, *J. Colloid and Interface Science* 177 (1996) 122–131.
- [37] A. Í. Vaizogullar, TiO<sub>2</sub>/ZnO Supported on Sepiolite: Preparation, Structural Characterization, and Photocatalytic Degradation of Flumequine Antibiotic in Aqueous Solution, *Chem. Eng. Commun.* 204 (6) (2017) 689-697.
- [38] A.L. Giraldo, G. A. Peñuela, R. A. Torres-Palma, N. J. Pino, R. A. Palominos, H. D. Mansilla, Degradation of the antibiotic oxolinic acid by photocatalysis with TiO<sub>2</sub> in suspension, *Water Res.* 44 (2010) 5158 -5167.
- [39] R.A. Palominos, A. Mora, M.A. Mondaca, M. Pérez-Moya, H.D. Mansilla, Oxolinic acid photo-oxidation using immobilized TiO<sub>2</sub>, *J. Hazard. Mater.* 158 (2008) 460–464.
- [40] H. Fang, Y. Gao, G. Li, J. An, P.-K. Wong, H. Fu, S. Yao, X. Nie, T. An, Advanced Oxidation Kinetics and Mechanism of Preservative Propylparaben Degradation in Aqueous Suspension of TiO<sub>2</sub> and Risk Assessment of Its Degradation Products, *Environ. Sci. Technol.* 47 (2013) 2704–2712.
- [41] Y. Nakabayashi, Y. Nosaka, •OH radical formation at distinct faces of rutile TiO<sub>2</sub> crystal in the procedure of photo electrochemical water oxidation, *J. Phys. Chem. C* 117 (2013) 23832–23839.
- [42] W. Song, W. Chen, W.J. Cooper, J. Greaves, G.E. Miller, Free-radical destruction of -Lactam antibiotics in aqueous solution, *J. Phys. Chem. A* 112 (2008) 7411–7417.
- [43] N. Lu, Y. Lu, F. Liu, K. Zhao, X. Yuan, Y. Zhao, Y. Li, H. Qin, J. Zhu, H<sub>3</sub>PW<sub>12</sub>O<sub>40</sub>/TiO<sub>2</sub> catalyst-induced photodegradation of bisphenol A (BPA): Kinetics, toxicity and degradation pathways, *Chemosphere* 91 (2013) 1266–1272.
- [44] S. Rong, Y. Sun, Degradation of TAIC by water falling film dielectric barrier discharge - Influence of radical scavengers, *J. Hazard. Mater.* 287 (2015) 317–324.
- [45] R.H. Schuler, P. Neta, R.W. Fessenden, Electron spin resonance study of the rate constants for reaction of hydrogen atoms with organic compounds in aqueous solution, *J. Phys. Chem.* 75 (1971) 1654–1666.
- [46] Y.X. Chen, S.Y. Yang, K. Wang, L.P. Lou, Role of primary active species and TiO<sub>2</sub> surface characteristic in UV illuminated photodegradation of Acid Orange 7. *J. Photochem. Photobiol. A: Chem.* 172 (2005) 47-54.
- [47] C. Richard, F. Bosquet, J.-F. Pilichowski, Photocatalytic transformation of aromatic compounds in aqueous zinc oxide suspensions effect of substrate concentration on the distribution of products. *J. Photochem. Photobiol. A: Chem.* 108 (1997) 45-49.
- [48] L. Ismaila, A. Rifai, C. Ferronato, L. Fine, F. Jaber, J.-M. Chovelon, Towards a better understanding of the reactive species involved in the photocatalytic degradation of sulfaclozine, *Appl. Catal. B: Environ.* 185 (2016) 88-99.
- [49] S. Rtimi, J. Nescic, C. Pulgarin, R. Sanjines, M. Bensimon, J. Kiwi, Effect of surface pretreatment of TiO<sub>2</sub> films on interfacial processes leading to bacterial inactivation in the dark and under light irradiation, *Interface Focus* 5 (2015) 1-12.
- [50] M. J. Uddin, F. Cesano, F. Bonino, S. Bordiga, G. Spoto, D. Scarano, A. Zecchina, Photoactive TiO<sub>2</sub> films on cellulose fibres: synthesis and characterization. *J. Photochem. Photobiol. A: Chem.* 189 (2007) 286–294.
- [51] B. R. Wang, K. Hashimoto, A. Fujishima, M. Chikuni, E. Kojima, A. Kitamura, M. Shimohigoshi, T. Watanabe, Photogeneration of Highly Amphiphilic TiO<sub>2</sub> Surfaces. *Adv. Mater.* 10 (2) (1998) 134-138.

- [52] S. H. Othman, S. A. Rashid, T. Idaty M. Ghazi, N. Abdullah, Dispersion and Stabilization of Photocatalytic TiO<sub>2</sub> Nanoparticles in Aqueous Suspension for Coatings Applications. *J. Nanomater.* (2012) 1-10.
- [53] T. K. Ghorai, P. Dhak, New synthetic approach, mesoporous properties and photocatalytic activity of titania adapted chromium-niobate nanocatalysts. *Adv. Mat. Lett.* 4(2) (2013) 121-130.
- [54] T.V. Edelio, C. B. Gustavo, C. T. Galo, Synthesis and Characterization of New Arylamine Chitosan derivatives. *J. Appl. Polymer. Sci.* 91 (2003) 807-812.
- [55] B. D. Mistry, *A Handbook of Spectroscopic Data Chemistry (UV, IR, PMR, <sup>13</sup>CNMR and Mass Spectroscopy)*, Oxford Book Co., Jaipur (2009) 39 p.

ACCEPTED MANUSCRIPT

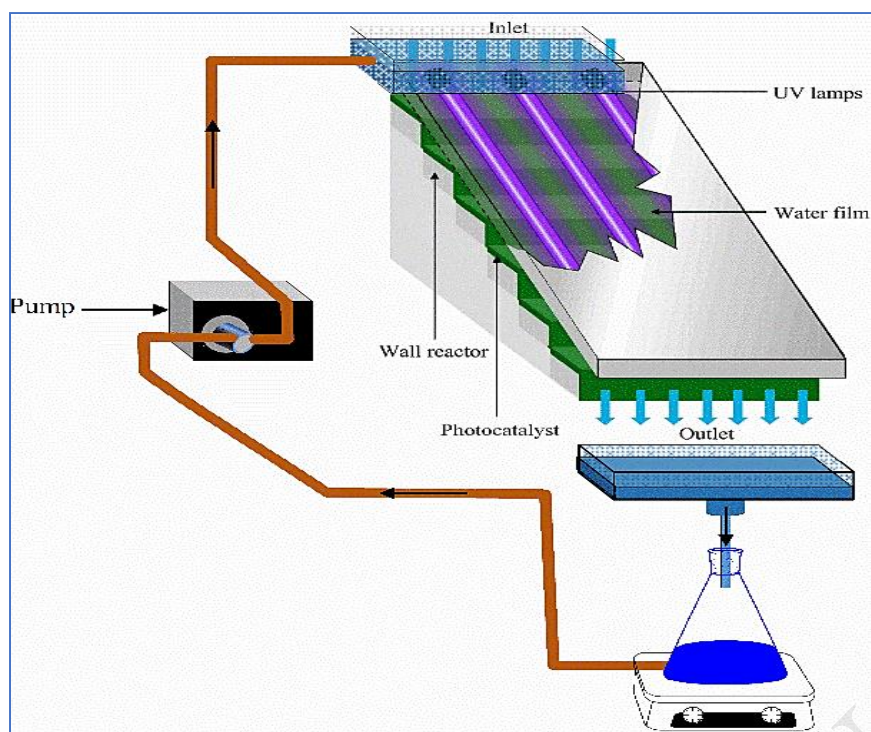


**Figure 1.** Experiment tool composition: pump, UV lamp, photocatalyst. The dark arrow denotes the water circulation.

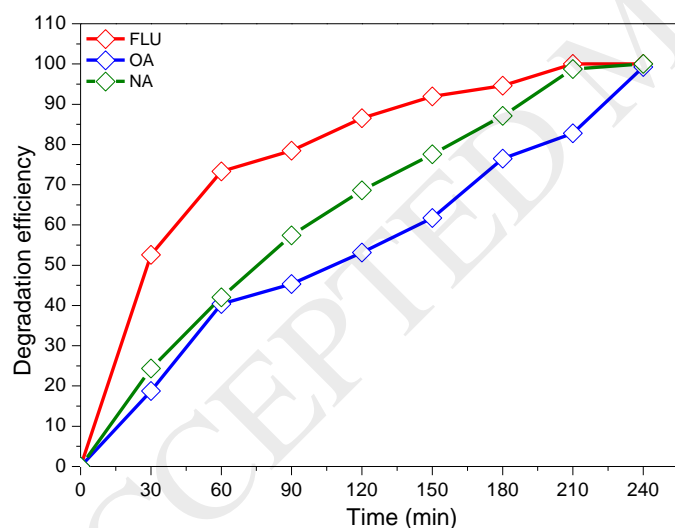


**Figure 2.** Individual degradation efficiency of FLU, OA, and NA with  $5 \text{ mg L}^{-1}$  initial concentration and  $2.6 \text{ g L}^{-1}$  catalyst dosage at  $\text{pH} = 7 \pm 0.1$ .

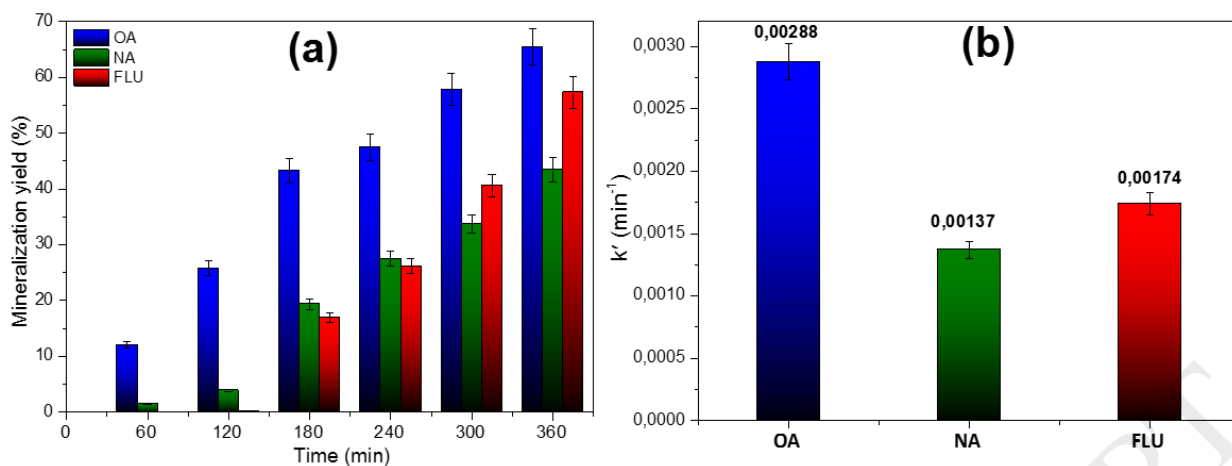


**Figure 3.** Mineralization yield (a) and pseudo-first-order rate constant ( $k'$ , min<sup>-1</sup>) (b) of FLU, OA and NA during 360 min of reaction at pH = 7 ± 0.1 with 5 mg L<sup>-1</sup> as initial concentration and 2.6 g L<sup>-1</sup> catalyst dosage.

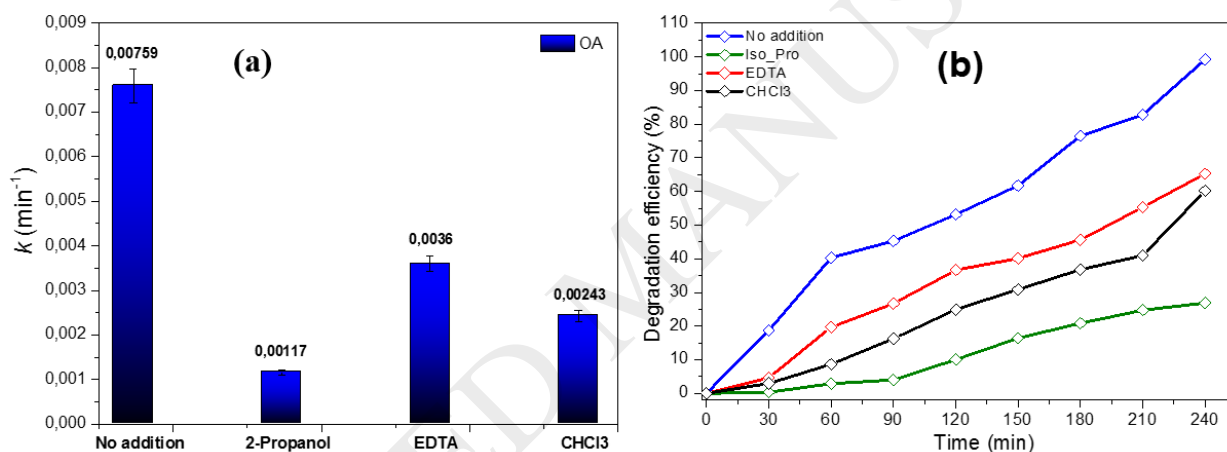


**Figure 4.** Effect of Isopropyl, EDTA and CHCl<sub>3</sub> on OA removal efficiency (b) and constant rate (a) using 2.6 g L<sup>-1</sup> of TiO<sub>2</sub>/cellulosic paper catalysts under UV light at pH = 7 ± 0.1: [OA] = [Iso-Pro] = [EDTA] = [CHCl<sub>3</sub>] = 5 mg L<sup>-1</sup>.

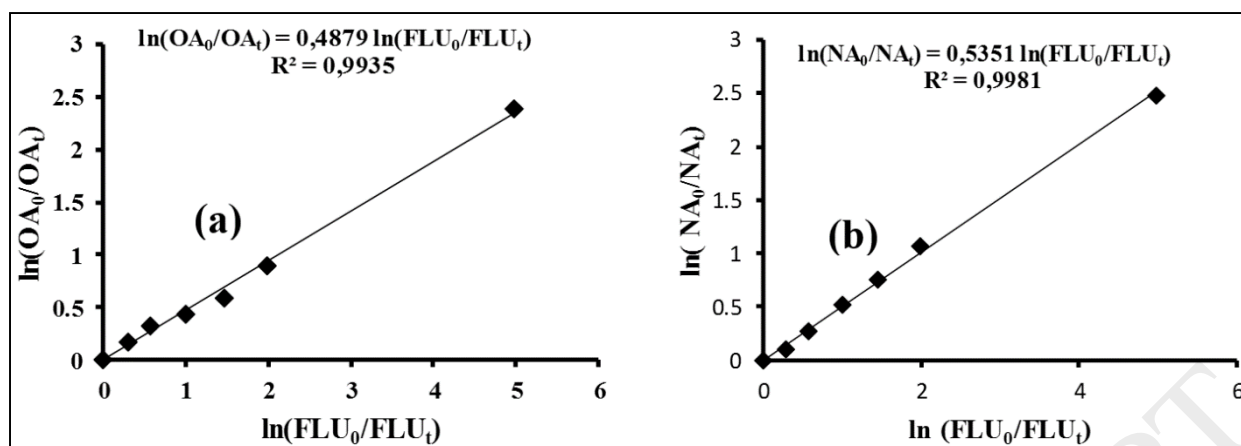


**Figure 5.** Determination method of second-order rate constant of (a) OA and (b) NA reacting with  $\cdot\text{OH}$  radicals.

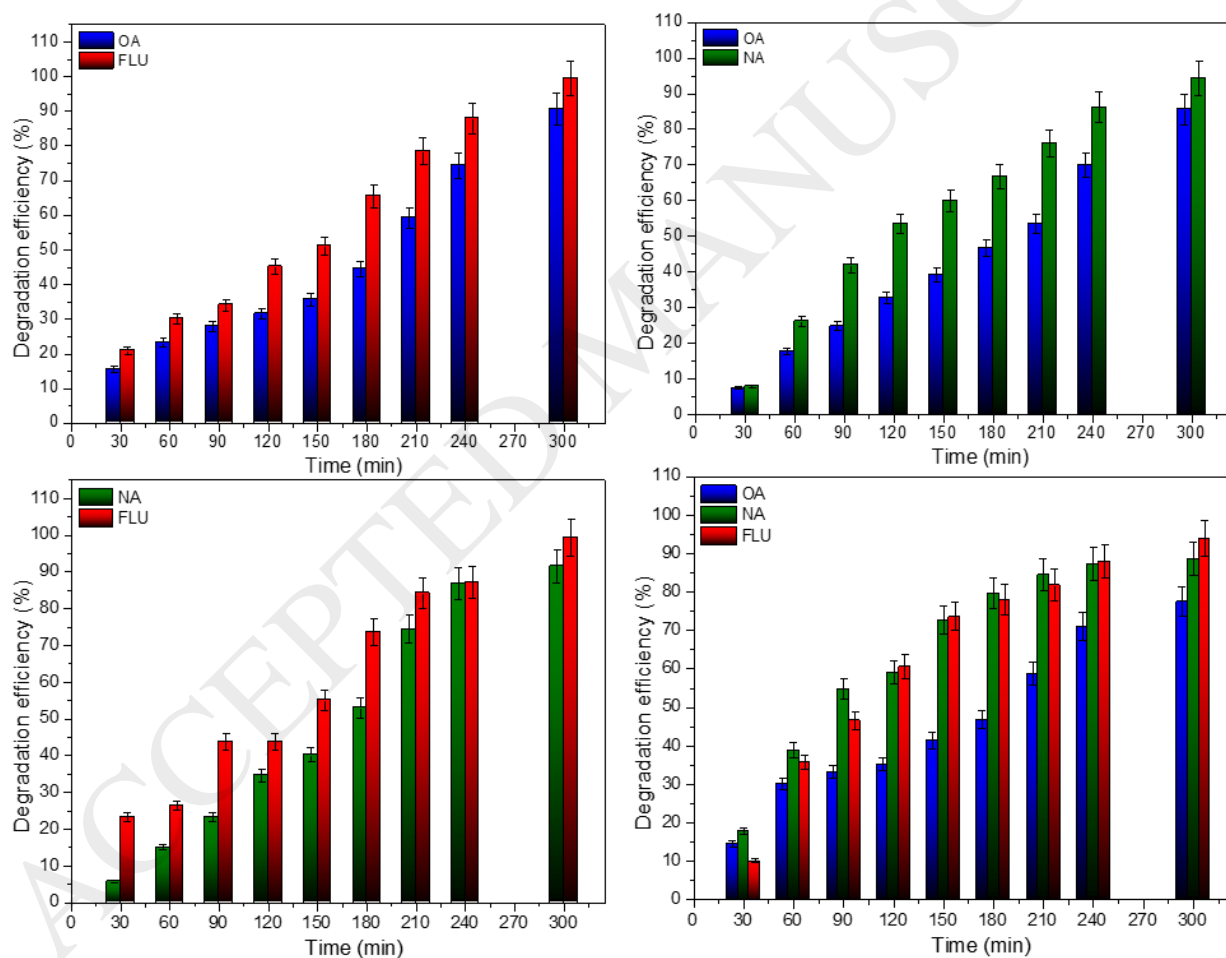


**Figure 6.** Photocatalytic degradation of FLU, OA and NA in binary and ternary systems with  $5 \text{ mg L}^{-1}$  as initial concentration of each antibiotic and  $2.6 \text{ g L}^{-1}$  catalyst dosage at  $\text{pH} = 7 \pm 0.1$ .

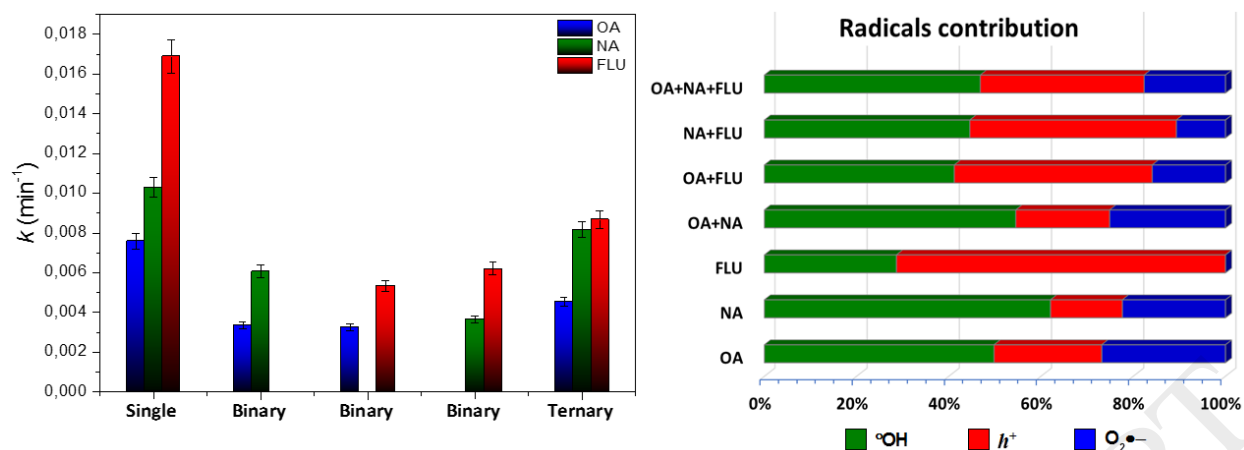


**Figure 7.** Pseudo-first-order rate constant and radicals implication percentages in mono-, binary- and ternary-compound systems with  $5 \text{ mg L}^{-1}$  as initial concentration of each antibiotic and  $2.6 \text{ g L}^{-1}$  catalyst dosage at  $\text{pH} = 7 \pm 0.1$  in 300 min.

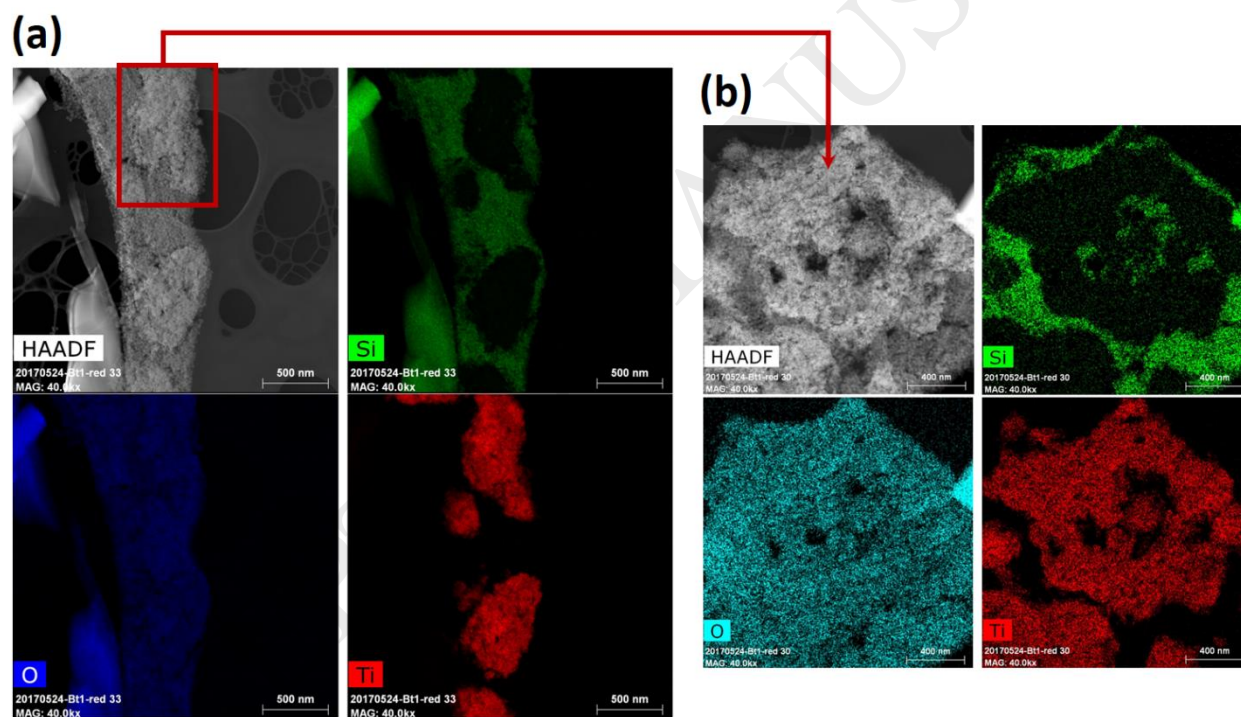


**Figure 8.** (a) HAADF coating distribution on the cellulose fiber fabrics. (b) HAADF distribution of elements and  $\text{SiO}_2$  binder role.

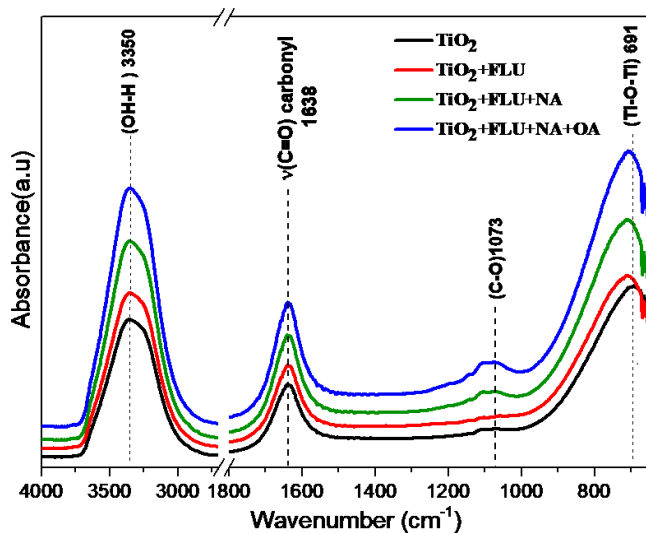


**Figure 9.** FTIR spectra before and after treatment of OA, NA, and FLU using mono-, binary- and ternary-compound(s) systems with  $5 \text{ mg L}^{-1}$  as initial concentration of each antibiotic and  $2.6 \text{ g L}^{-1}$  catalyst dosage at  $\text{pH} = 7 \pm 0.1$  in 300 min.

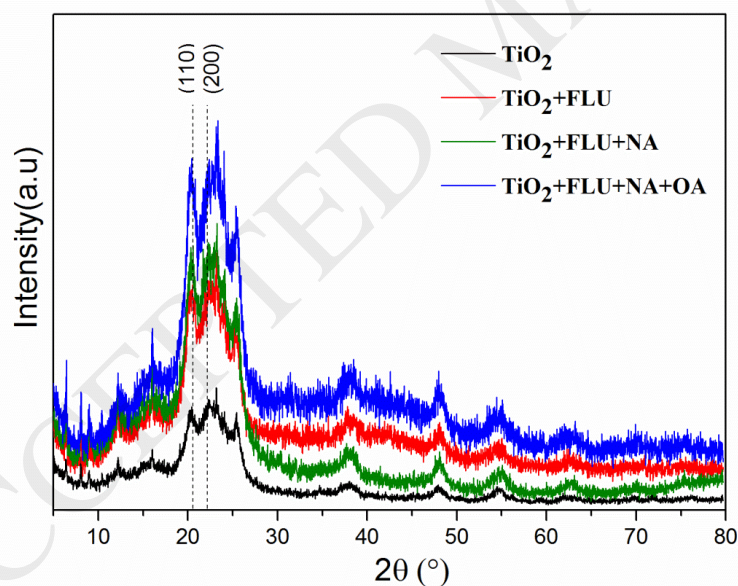


**Figure 10.** XRD patterns before and after treatment of OA, NA, and FLU using mono-, binary- and ternary-compound(s) systems with  $5 \text{ mg L}^{-1}$  as initial concentration of each antibiotic and  $2.6 \text{ g L}^{-1}$  catalyst dosage at  $\text{pH} = 7 \pm 0.1$  in 300 min.

**Table 1:** Physico-chemical properties and structure of antibiotics.

|                                | FLU   | OA  | NA  |
|--------------------------------|---|---|---|
| <b>Chemical formula</b>        | C <sub>14</sub> H <sub>12</sub> FNO <sub>3</sub>  | C <sub>13</sub> H <sub>11</sub> NO <sub>5</sub> | C <sub>12</sub> H <sub>12</sub> N <sub>2</sub> O <sub>3</sub> |
| <b>MW (g mol<sup>-1</sup>)</b> | 261.25  | 261.23  | 232.24  |
| <b>λ<sub>max</sub> (nm)</b>    | 246   | 268   | 258   |
| <b>Chemical structure</b>      | <p>The image displays three chemical structures side-by-side. From left to right: 1. FLU (Fluoroquinolone): A quinolone ring system with a fluorine atom at position 6, a methyl group at position 7, and a carboxylic acid group at position 4. 2. OA (Oxazolidinone): A benzimidazole ring system with a methyl group at position 2, a carboxylic acid group at position 4, and a fused oxazolidinone ring system. 3. NA (Naphthylisoquinoline alkaloid): A naphthylisoquinoline alkaloid with a methyl group at position 1, a carboxylic acid group at position 2, and a methyl group at position 8.</p> |   |   |